



Full Length Article

On formation of Al–O–C bonds at aluminum/polyamide joint interface

F.C. Liu^a, P. Dong^{a,b,*}, W. Lu^b, K. Sun^c^a Department of Naval Architecture and Marine Engineering, University of Michigan, Ann Arbor, MI 48109, USA^b Department of Mechanical Engineering, University of Michigan, Ann Arbor, MI 48109, USA^c Department of Materials Science and Engineering, University of Michigan, Ann Arbor, MI 48109, USA

ARTICLE INFO

Keywords:

Polyamide/nylon
 Aluminum alloys
 Dissimilar materials joining
 Joining mechanism
 X-ray photoelectron spectroscopy
 Friction stir welding

ABSTRACT

Strong dissimilar materials joints consisting of aluminum alloy and polyamide 66 (PA66) plates were produced by a new joining method: friction lap welding (FLW). To understand the key joining mechanism, special samples were made by evaporation of aluminum oxide onto PA66 plates to form an aluminum alloy/PA66 interface. X-ray photoelectron spectroscopy (XPS) was used for characterizing the resulting interfacial chemistry in these aluminum alloy/PA66 samples. Both the Al2p and C1s spectra of XPS confirmed the formation of Al–O–C bonds at the interface between PA66 and alumina coating. Approximately 23.6% of the Al atoms in the 0.8 nm alumina coating have contributed to the formation of Al–O–C bonds. The carbonyl group at the PA66 surface played an essential role in the formation of such an Al–O–C bond. The formation of Al–O–C bonds was proved to be a key factor for achieving good joint strengths in such metal/polymer joints, providing a direct understanding why aluminum alloys can be directly welded to PA66 plates with superior joint strength.

1. Introduction

Thermoplastic composites possess high specific strength, good formability, low processing cost, and good recyclability. Use of thermoplastic composites in aircraft, automotive, rail transport, and watercraft structures has grown rapidly over the last decade as increasingly stringent structural light weighting requirements continue to dominate the design and manufacture of modern transportation vehicles. There is a growing demand for developing reliable plastic/metal joining processes for high volume production. Conventional adhesive bonding processes require a long curing time, and the adhesives are susceptible to environmentally induced degradation for some applications [1,2]. Mechanical fastening introduces additional weights and may not be suited for achieving hermetic sealing or pressure containment under certain conditions. As a result, various plastic/metal welding processes have been explored recently in some forms of hybrid joints [3–6] that may possess joint strengths that cannot be explained by macroscopic or microscopic mechanical interlocking. These joining processes involved local melting at the plastic/metal joint interface with different heating sources, such as friction [3–5,7,8], laser beam [6,9–11], ultrasonic vibration [12,13], electric joule heating [14], and induction heating [15]. Among these processes, friction stir lap welding (referred to as friction lap welding or FLW in [3–5,16]) has shown a great promise due to its process simplicity and easiness in achieving

automation for high-volume production.

The concept of FLW is illustrated in Fig. 1a. A non-consumable cylindrical tool is first set to rotate at a desirable speed and moved to press against the metal sheet sitting on top of the thermoplastic composite part. Once the desired pressure and temperature are attained, the cylindrical tool is set to travel along the welding direction at a fixed speed. The primary function of the cylindrical tool is to generate frictional heat while exerting a sufficient local pressure to form a sound joint between the plastic and metal piece. Localized heating and melting at the plastic/metal interface is accomplished by the conduction of friction heating. A good bond forms at the interface after the melted plastic solidifies under pressure.

A friction lap welded specimen between Nylon and 6061 Al is shown in Fig. 1b (tool rotational speed: 2000 rpm; travel speed: 800 mm/min, and tool plunge depth: 0.34 mm). Tensile-shear tests showed that failures occurred across the nylon sheet along joint fillet location instead of along the joint interface (Fig. 1c), indicating that a strong bond is present at the joint interface. Scanning electron microscopy examination showed that Nylon and the 6061 Al are tightly bonded together (Fig. 1d), with no clear indication that mechanical interlocking has played a major role in the strong bond strengths demonstrated from the tensile-shear test results. Then, what could be the possible bonding mechanisms? This is a fundamental question that needs to be addressed in order to effectively guide the development of a

* Corresponding author. Tel.: +1 734-615-7484.

E-mail address: dongp@umich.edu (P. Dong).<https://doi.org/10.1016/j.apsusc.2018.10.024>

Received 22 August 2018; Received in revised form 30 September 2018; Accepted 3 October 2018

Available online 04 October 2018

0169-4332/ © 2018 Elsevier B.V. All rights reserved.

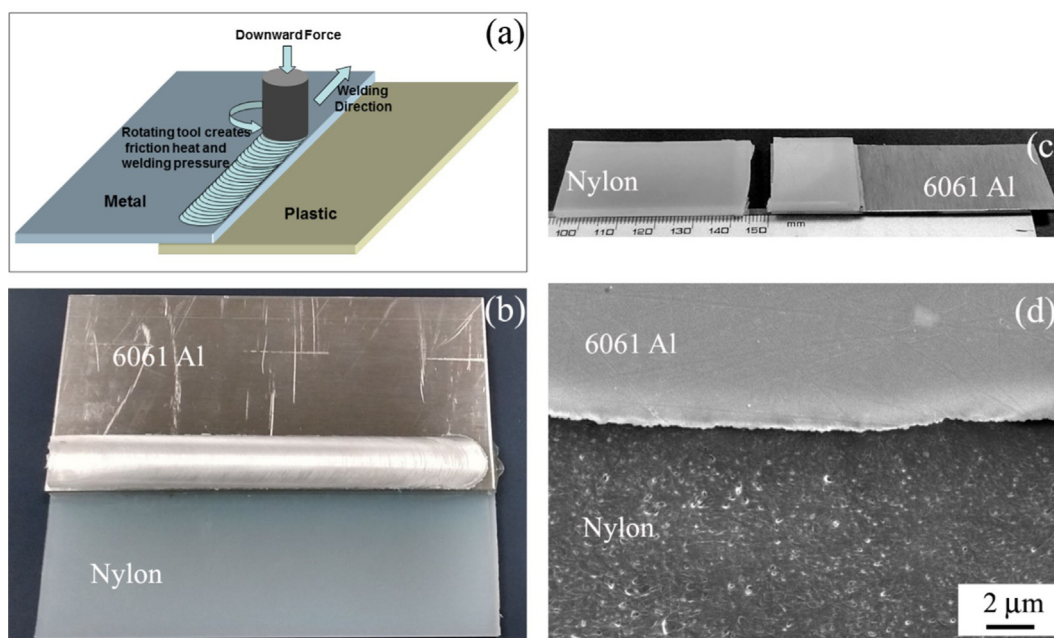


Fig. 1. Schematic illustration of FLW process (a); as-welded FLW 6061 Al/nylon dissimilar-material weld (b); typical failed tensile test FLW sample (c); and SEM cross sectional observation of FLW sample.

robust joining process for achieving reliable bonds between polymer and metal.

Some earlier exploratory investigations showed that sheets of polyamide (PA or nylon) [3,5], polyethylene terephthalate (PET) [6,17], polycarbonate (PC) [18], and polymethylmethacrylate (PMMA) [19] could be directly welded onto metal plate surfaces through a local melting of polymers against metal interface under pressure. All these polymers contain carbonyl groups (C=O). In contrast, the thermal plastics without carbonyl groups, such as polyethylene (PE) [4,16], polypropylene [4], polystyrene (PS) [20], and polyvinyl chloride (PVC) [21], cannot be welded to metals without a proper surface pre-modification. When carbonyl groups were grafted onto the PE surface by the corona discharge treatment [16], strong hybrid welds between PE and metal were produced [4,16]. The investigations described above indicated that the carbonyl group (C=O) was highly effective for developing a form of chemical bond in polymer/metal joints.

In practice, almost all available Al plates for engineering applications are covered by alumina. This is because the formation of the first monolayer of alumina on Al alloy surface is virtually instantaneous, depending only on the arrival rate of oxygen from the environment. One plausible theory is that an aluminum/polymer welding could be achieved through the formation of chemical bonds between alumina and polymer. To the best of our knowledge, no work has been done in proving such a bond formation between alumina and PA 66 at the joint interface.

X-ray photoelectron spectroscopy (XPS) has been shown as a valuable tool for characterizing chemical reactions at the metal/polymer interface [22–26]. The typical spatial resolution of XPS is larger than several tens of micro meters while the interfacial reaction layer of metal/polymer welds could be as thin as 1 nm (2–3 layer of atoms). Thus, interfacial chemical bonds cannot be discerned through a cross-sectional XPS examination of the metal/polymer welds due to the low proportion of retraction layer in an XPS spot. In addition, a typical XPS analysis depth is about 3–10 nm. It is very difficult to precisely thin down either the metal or the polymer plates of metal/polymer joints to that size. Therefore, a great deal of difficulties exists in using XPS for determining the interfacial chemistry in polymer/aluminum joints.

To solve this problem, an alumina layer with thicknesses varying from 1 to 15 nm was deposited onto polyamide 66 (PA66) plates

through a physical vapor deposition (PVD) process in this study. This allows a precise examination of the chemical bonds developed at the PA66/alumina interface using XPS. Regarding whether such a PVD sample yields representative interfacial chemical bonds of the PA66/aluminum joints referred to earlier, a recent investigation has already showed that the joining strength of the PA66/aluminum joints was not affected by the welding temperature as long as the temperature is high enough to locally melt the PA66 at the joining interface [8]. This suggests that process temperature is not a critical factor for developing interfacial chemical bonds between PA66 and alumina, as long as local melting of the nylon can be attained for establishing an intimate atomic contact at the interface. Therefore, the present study aimed at understanding the joining mechanisms between aluminum and polymer using a simulated PVD sample under controlled conditions.

2. Experimental details

1.98 mm thick off-white commercial PA66 sheet was used as base materials in this study. The quality of the nylon sheet meets specifications of ASTM D5989 and ASTM D6779. The tensile strength of the nylon plate is 77 MPa. Small PA66 plates (15 × 15 × 2 mm) were cut from the PA66 sheet for alumina deposition and cleaned with ultrasonic washer for 20 min, and then were dried in an oven at 70 °C for 96 h to desorb moisture. Alumina was deposited onto the PA66 surface in a vacuum chamber (base pressure of 4×10^{-4} Pa) by magnetron sputtering. An alumina target (99.9995% purity) was fixed on a magnetron cathode with a working distance of ~180 mm from the substrate. Alumina was sputtered using an argon plasma under a pressure of 0.4 Pa and an RF power of 175 W. The average deposition rate was determined to be 0.48 nm/min at the investigated condition. Various thickness of alumina can be achieved by controlling the deposition time.

The PA66 plates with alumina coating were taken into another laboratory for XPS analysis. Despite that special care was taken during sample transfer between locations (using vacuum sealer bags), brief contact with room atmosphere could not be totally avoided during the process of unloading sample from the deposition vacuum chamber and loading sample into the XPS vacuum chamber. To remove possible surface contaminations, the alumina surface was sputtered by pure

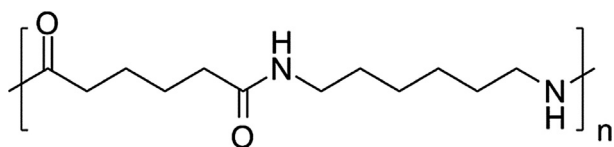


Fig. 2. Structural formula of PA66.

argon ion beam for 10 s in the XPS vacuum chamber prior to XPS measurement. About 0.2 nm thick alumina was removed by the ion beam sputtering.

XPS experiments were carried out in a Kratos Axis Ultra XPS system using monochromatic Al X-ray source at room temperature. During measurement, the pressure in the analysis chamber was in the range of 3×10^{-6} – 1×10^{-7} Pa. A charging compensation was applied during data acquisition, and all the spectra were calibrated by setting the C1s hydrocarbon peaks and Al2p Al_2O_3 peaks to the positions of binding energy of 285.0 eV and 74.6 eV, respectively. All the data were analyzed by the Casa XPS software using the Shirley type background.

3. Results and analysis

As shown in Fig. 2, two carbonyl groups ($\text{C}=\text{O}$) are present out of every 12 carbons along the chains of PA66. To identify the change in surface chemical state of PA66 before and after the alumina deposition, one clean PA66 plate was measured by XPS prior to alumina deposition. The XPS survey spectra (0–600 eV) of the clean PA66 is shown in Fig. 3a. Only O1s, N1s and C1s peaks were evident. The atomic percentages of O1s, N1s and C1s were listed in Table 1. The XPS results showed that the relative content of O, N and C at the PA66 surface was in good agreement with the structural formula of PA66 (Fig. 2), except for a small amount of extra C atoms.

Fig. 3b shows the C1s spectrum of the clean PA66 plate. The best fit for decomposition was achieved when a Full width at half maximum (FWHM) of 1.3 eV was used for each component. The C1s spectrum of the clean PA66 was fitted using four distinct components: (1) Carbon involved in the C–C and C–H bonds of PA66 (285.0 eV) was expressed as C–C; (2) Carbon located between CH_2 groups and nitrogen atoms was represented as C–N (286.3 ± 0.1 eV); (3) $\text{C}=\text{O}$ referred to the carbon in the carbonyl group (288 ± 0.1 eV); (4) Carbon in carboxylic acid groups COOH ($\text{O}-\text{C}=\text{O}$) was also detected at 289.3 ± 0.1 eV, indicating that the PA66 chains contain non-condensate carboxylic acid end groups. The relative content of each type of components was determined according to the area under the corresponding components

Table 1
Chemical atomic composition obtained through XPS scan on clean PA66 (without considering hydrogen atoms) and 15 nm thick alumina coating.

Sample	O1s (at. %)	N1s (at. %)	C1s (at. %)	Al2p (at. %)
PA66	11.8	9.7	78.5	–
Alumina Coating (15 nm)	58.7	–	–	41.3

Table 2
Fitting parameters of C1s spectra and proportion of resolved components obtained from clean PA66 and PA66 with various thickness of coating.

		C–C	C–N	C=O	C–O–Al	O–C=O
Clean PA66	FWHM (eV)	1.30	1.30	1.30	–	1.30
	Binding energy (eV)	285	286.3	288	–	289.3
	Atomic percentage (%)	72.3	14.2	12.7	–	0.8
PA66 with 0.8 nm Alumina coating	FWHM (eV)	1.50	1.50	1.50	1.50	1.50
	Binding energy (eV)	285	286.3	287.9	284	289.3
	Atomic percentage (%)	71.2	15.9	6.5	4.9	1.5
PA66 with 3.2 nm Alumina coating	FWHM (eV)	1.50	1.50	1.50	1.50	1.50
	Binding energy (eV)	285	286.4	288.1	284	289.4
	Atomic percentage (%)	69.9	16.4	5.6	6.8	1.3

(Fig. 3b). The results were summarized in Table 2, showing that the relative ratio of each component is consistent with the structural formula of PA66 excluding a slight C–C enrichment (6% relative). The additional C–C observed can be attributed to the presence of additives used in the extrusion process of PA66 sheets and the surface hydrocarbon contamination from the environment during storage. It should be noted that the maximum thickness probed by XPS is approximately 4–5 nm [24] and the outermost monolayer emits the highest volume of photoelectron comparing to other layers. Thus even a very small fraction of monolayer contamination on sample surface can be detected by XPS and the measured contamination content is larger than the actual content. However, such a small volume of contamination will not likely significantly affect the chemical bonds at the PA66 surface.

To determine the FWHM of the Al2p peak of alumina, a PA66 plate with 15 nm thick alumina deposition was analyzed by XPS. Only the

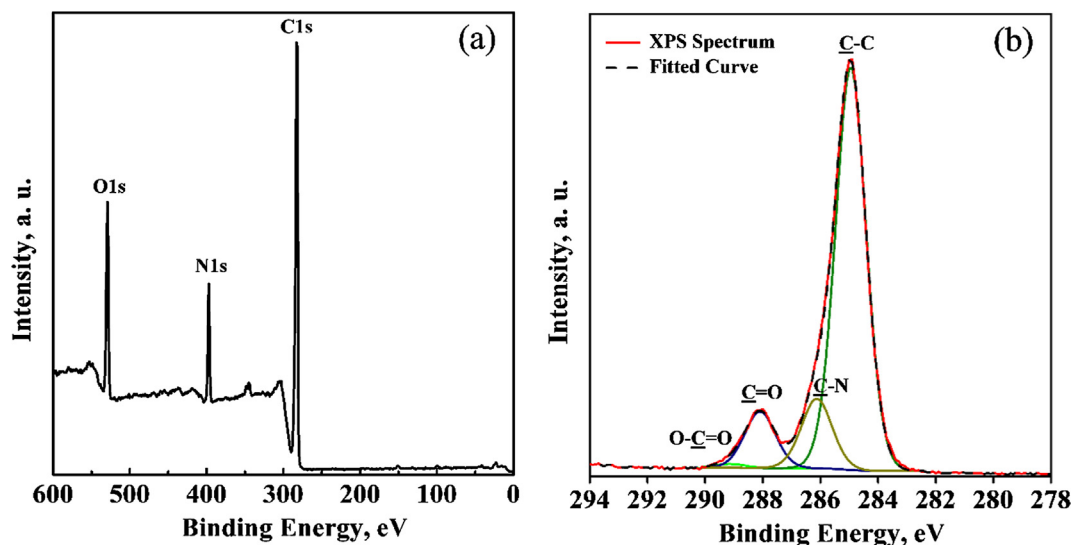


Fig. 3. XPS survey spectrum (a) and C1s core level spectrum (b) of as-received PA66.

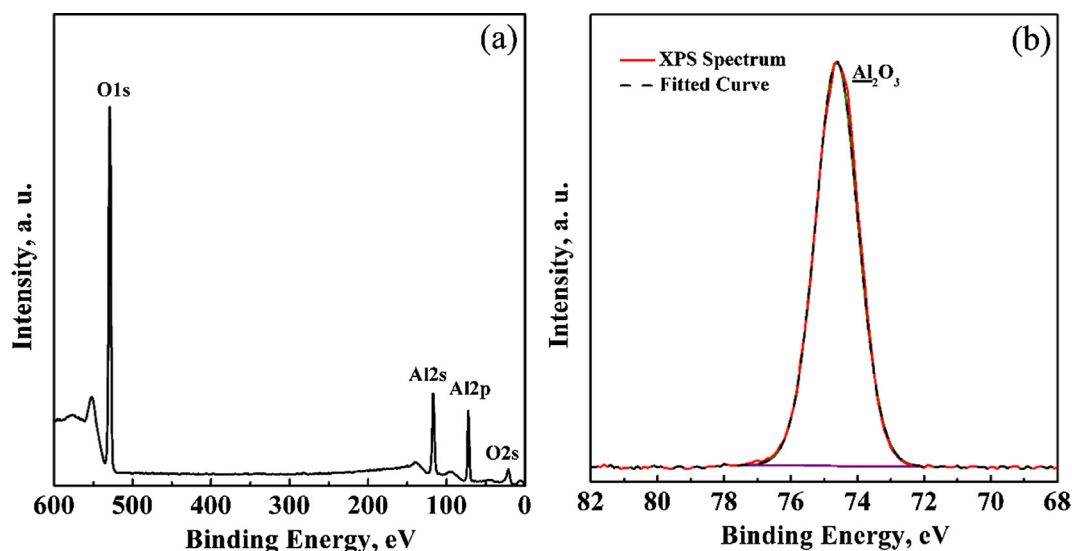


Fig. 4. XPS survey spectrum (a) and Al2p core level spectrum (b) from a 15 nm thick Al₂O₃ coating on PA66 plate.

peaks of O1s, Al2s, Al2p and O2s were visible in the XPS survey (Fig. 4a). The absence of C and N peaks indicated no photoelectron emitted from PA66 had penetrated the alumina coating. The atomic percentage of O1s and Al2p (Table 1) are consistent with the content of O and Al atoms in Al₂O₃, confirming that pure Al₂O₃ was deposited on the PA66 surface. The analysis results above indicated that the Al2p spectrum in Fig. 4b is solely the result of the Al atoms in Al₂O₃ coating. Therefore, only a single component Al₂O₃, in which Al atoms are linked to oxygen, was resolved from the Al2p spectrum at 74.6 eV. The FWHM of this component is 1.5 eV.

Fig. 5 shows the XPS survey spectra (0–600 eV) as a function of alumina coating thickness. It clearly shows that O1s, Al2s, and Al2p intensities declined while emission signals of N1s and C1s became stronger with decreasing thickness in alumina coating. The attenuation of O1s, Al2s, and Al2p intensities with thinner alumina coating is ascribed to less alumina to emit photoelectrons. The intensification of N1s and C1s peaks can be explained by the screening effect, that is more photoelectrons come from the PA66 surface have penetrated the thinner alumina coating.

The atomic percentage of O1s, N1s and C1s and Al2p obtained from each XPS survey is listed in Table 3. According to the chemical formula of PA66, the atomic ratio of N/C should be 0.167. However, the XPS result showed the atomic ratio of N/C on the PA66 surface is in the range of 0.145–0.148. This discrepancy could be attributed to hydrocarbon contamination on the PA66 surface.

The O1s peak in Fig. 5a was attributed to the O atoms in both Al₂O₃ coating and the C=O groups in PA66. The structural formula of PA66 indicated that the atomic content of O and N in PA66 is equal. Therefore, the content of O atoms in Al₂O₃ can be estimated by O1s-N1s (at. %). The atomic ratio of O/Al in alumina coating can be estimated by (O1s-N1s)/Al2p. The results are summarized in Table 3, showing a deficit of O atoms in the Al₂O₃ coating. The loss of O atoms may be associated with the ion beam sputter prior to XPS scanning. It appears that O atoms were easier to be knocked off from alumina by the ion beam than Al atoms.

Fig. 6 shows the fitted Al2p spectra obtained from the PA66 plates with a varying thickness of the alumina coating. The fitting parameters are present in Table 4. The FWHM of all the resolved components from Al2p spectra is 1.5 eV (Table 4). Fig. 6a shows that in addition to the component of Al₂O₃ at 74.6 eV, a distinct component at 75.2 eV also appeared in the Al2p spectrum of the sample with 3.2 nm Al₂O₃ coating. This new component was in the form of Al–O–C bonds and expressed as Al–O–C. Another new component at 73.0 eV was

observed only in the spectra collected from the samples with 1.5 nm and 0.8 nm alumina coating (Fig. 6b and c). This new component involving Al atoms linked to C atoms directly was denoted as Al–C.

Al–C bond only appeared in the XPS spectrum when alumina coating was thinner than 1.5 nm. The highest fraction of the Al–C bond (2.9%) was obtained in the PA66 sample with 0.8 nm thick alumina coating. It was less than 14.3% of the volume of Al–O–C bonds in the same sample. There are two possibilities for the Al–C bonds formation. The first one is that a very low volume of Al–C bond formed during alumina deposition. The second one is that the ion beam sputtering of alumina surface promoted the Al–C bond formation.

An increased proportion of Al–O–C and Al–C components were detected when the alumina coating became thinner (Fig. 6 and Table 4), demonstrating the Al–O–C and Al–C bonds formed at the PA66/alumina interface. These bonds should be mainly situated between the monolayers of alumina and PA66 at the interface if the atoms penetration in PA66 is trivial. Theoretically, the fraction of Al–O–C and Al–C components should continue to increase with a decrease in alumina thickness. As ion beam sputter was applied in this study to remove surface contaminations, there was a concern that the ion beam sputter may affect the chemical bonds at the interface if the coating is too thin. Therefore, the thinnest alumina coating investigated in the present study is 0.8 nm thick (about 3–4 layer of Al atoms). Table 4 showed that approximately 23.6% of the Al atoms in the 0.8 nm alumina coating have contributed to the Al–O–C bonds. All the Al2p spectra in Fig. 6 have shown that the dominant new bond developed across the interface of PA66/alumina is of the Al–O–C type.

The fitted C1s spectra obtained from the PA66 plates with 3.2 and 0.8 nm thick alumina coating are shown in Fig. 7. The fitting parameters of the resolved components are presented in Table 2. The FWHM of all the resolved components is 1.5 eV. Compared to the components obtained from the clean PA66, the proportion of C=O components decreased noticeably. A new component at 284 eV caused by the formation of C–O–Al bonds was detected and was expressed as C–O–Al. Table 2 shows that the decrease of C=O components from the amide groups was compensated by the new C–O–Al components in both samples. These results demonstrated the carbonyl groups from the amide groups were the primary reaction sites for developing C–O–Al bonds.

The diminishing of C=O components became more noticeable in the sample covered by 3.2 nm alumina (Fig. 7 and Table 2). This is because the C1s spectrum of the PA66 plate with 3.2 nm alumina coating contains a higher proportion of photoelectrons emitted from the

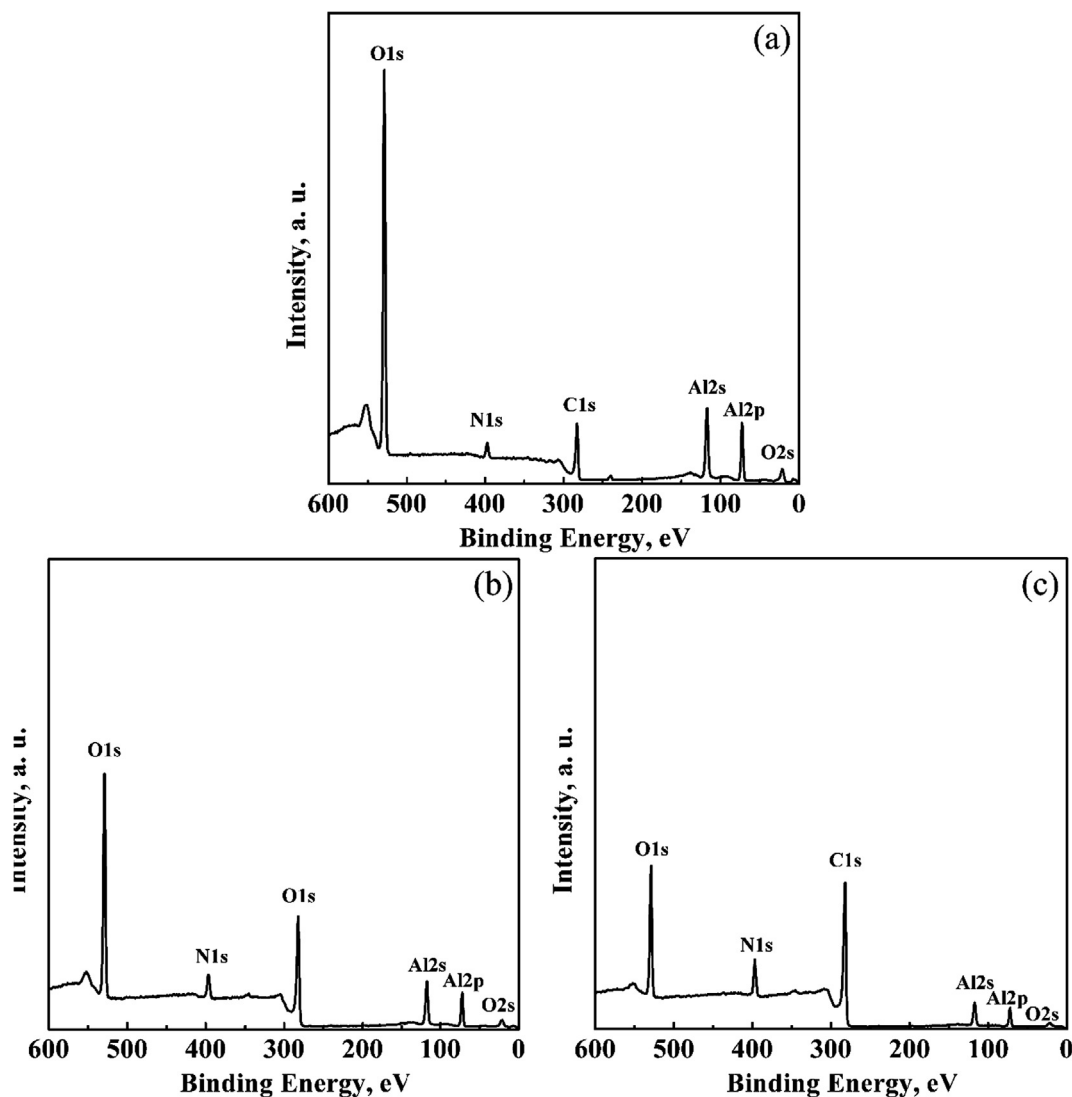


Fig. 5. XPS survey spectra (0–600 eV) as a function of Al_2O_3 coating: (a) 3.2 nm (b) 1.6 nm and (c) 0.8 nm.

Table 3

Chemical atomic composition obtained through XPS scan on PA66 with various thickness of coating (without considering hydrogen atoms).

Alumina thickness	O1s (at%)	N1s (at%)	C1s (at%)	Al2p (at%)	N1s/C1s (at%)	(O1s-N1s)/Al2p (at%)
3.2 nm	45.45	3.25	22.10	29.20	0.147	1.45
1.5 nm	32.84	5.98	41.28	19.90	0.145	1.35
0.8 nm	20.69	8.86	59.67	11.08	0.148	1.09

surface monolayer of PA66. Fig. 7 also showed that the difference between the two samples regarding the content of $\text{C}=\text{O}$ components is small. This may be attributed to the fact that the reaction between PA66 and alumina deposition was not limited to the first monolayer. A certain extent of atom penetration into PA66 cannot be completely avoided during PVD deposition. It is interesting to note that C–Al bond ($282 \pm 0.2 \text{ eV}$) was not detected by the C1s spectra (Fig. 7). This should be attributed to that the proportion of C–Al bonds is too low to be distinguished from the C1s spectra.

4. Discussions

This study has demonstrated that the carbonyl groups ($\text{C}=\text{O}$) were

the primary reaction sites for developing C–O–Al bonds across the PA66/alumina interface. With this fundamental understanding, it is now possible to highlight the importance of carbonyl in metal/PA66 welding from a new perspective by a systematic analysis of available studies in the literature.

The typical results from literature indicating potential chemical bonds that might have formed are summarized in Table 5. It shows that the weldability of metal/polymer hybrid joints is mainly determined by the type of polymer matrix involved. The thermal plastics of PA, PET, PEI, PC, and PMMA types which contain $\text{C}=\text{O}$ groups were shown weldable to various metals without needing special surface modification. Note that surfaces of Al alloys, Mg alloys, Ti alloys, stainless steel, and galvanized steel are typically covered by an oxidized layer prior to welding. An extrapolation from the XPS results of the present study indicates that the metal surface oxides could react with polymer during welding and form C–O–M bonds (note: “M” here denotes a metal atom).

The literature also showed that copper and carbon steel could be directly welded to PA or PET [7,16,27]. Copper and carbon steel takes a relatively long time to form surface oxides in the atmosphere. When the polished surface of such metal was welded against polymer, a clean metal surface was in contact with polymer directly. The chemical reaction of this kind of interface has been investigated [22,24]. XPS has been used to study the interface between an in-situ deposited Al or Cu

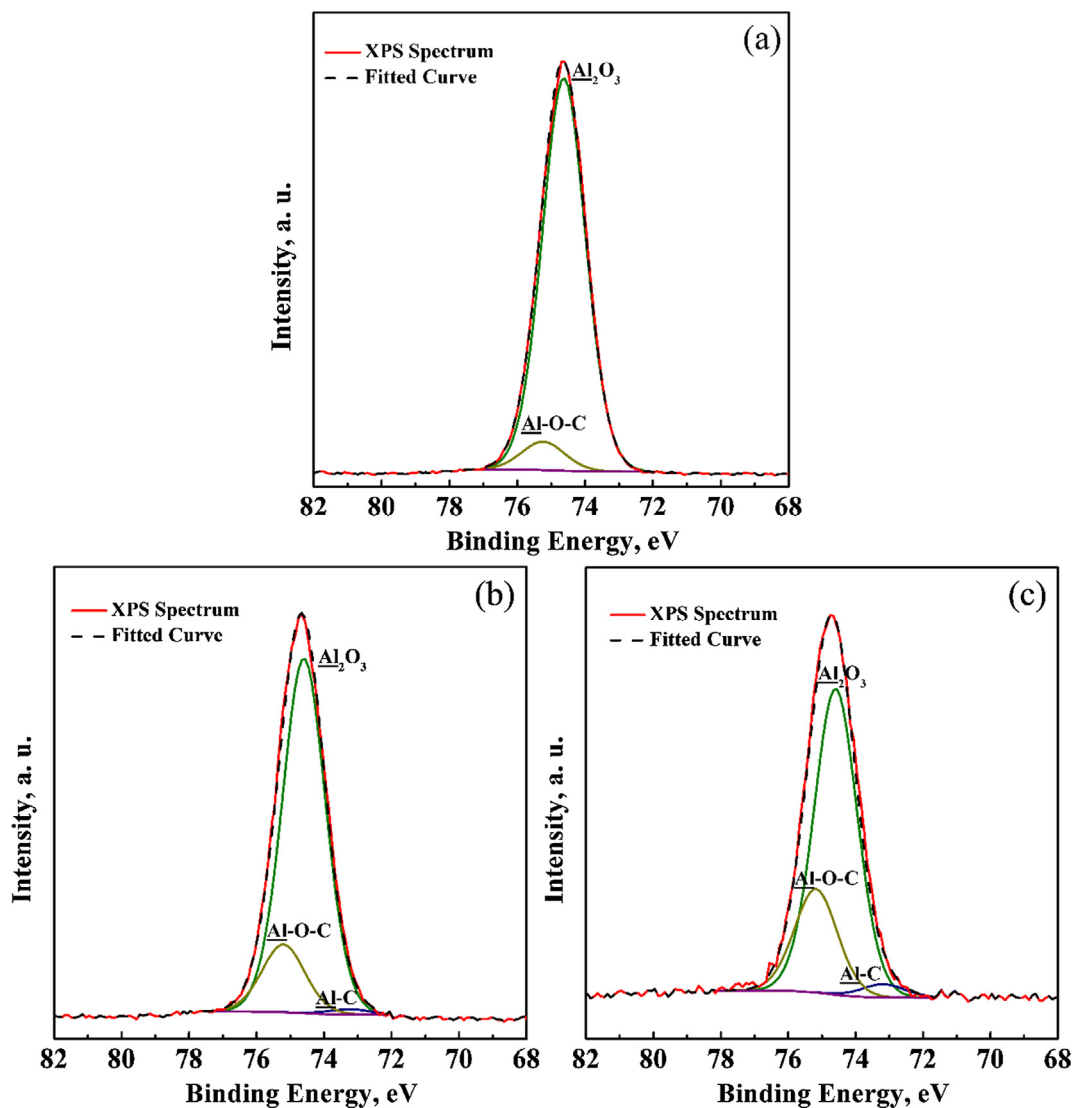


Fig. 6. Al₂p core level spectra recorded as a function of Al coating: (a) 3.2 nm (b) 1.6 nm and (c) 0.8 nm.

Table 4

Fitting parameters of Al₂p spectra and proportion of resolved components obtained from PA66 with various thickness of coating.

Alumina coating (nm)		Al ₂ O ₃	Al–O–C	Al–C
3.2	FWHM (eV)	1.50	1.50	–
	Binding energy (eV)	74.6	75.2	–
	Atomic percentage (%)	93.2	6.8	–
1.5	FWHM (eV)	1.50	1.50	1.50
	Binding energy (eV)	74.6	75.2	73.0
	Atomic percentage (%)	82.9	15.9	1.2
0.8	FWHM (eV)	1.50	1.50	1.50
	Binding energy (eV)	74.6	75.2	73.0
	Atomic percentage (%)	73.5	23.6	2.9

coating on PET film. Both Al and Cu have chemically interacted with PET to form interfacial compounds. Al–O–C compounds at the interface of deposited Al coating and PET film were detected by XPS [22,24]. The interaction of the PET film and Cu atoms was weaker, thus Cu atoms diffused into the PET matrix. Nevertheless, O₂ plasma of PET produced additional oxygenated species at the surface of PET film, limiting the diffusion of Cu atoms into PET by chemically trapping Cu atoms. As a result, C–O–Cu bonds formed at the surface of the Cu

coating and the treated PET film. These polymer metallization investigations have proved that C–O–M bonds could also develop at the interface between pure metal and polymer. Thus, C–O–M bonds are expected to have formed across the interface of copper/PA6 [7], copper/PET [27] and carbon steel/PA6 [14] during welding, contributing to the high strength of these hybrid joints.

Table 5 also showed that surface modifications were required to produce a strong bond in metal/polymer joints when PE, PP, ABS, PPS or PVC were the polymer matrices. The modifications can be made either on the polymer or metal surface. Through plasma treatment, corona discharge or acid-modification [4,14,22], C=O groups can be implanted or grafted on PE or PP, allowing C–O–M bonds being formed across the joint interface. The metal surface modification can be achieved through plasma electrolytic oxidation [4], high-temperature oxidation [28], or laser texturing [29]. The goal is to generate micro holes or textures on the metal surface. So that the joining could be enhanced by micro mechanical interlocking [21].

Combining the present investigation and the literature, we concluded that C–O–M bonds can form at the interface of either metal oxide/polymer or metal/polymer. The carbonyl groups at polymer surface play an important role in developing C–O–M bonds at the interface.

Our new understanding of the chemical bonding can also help to

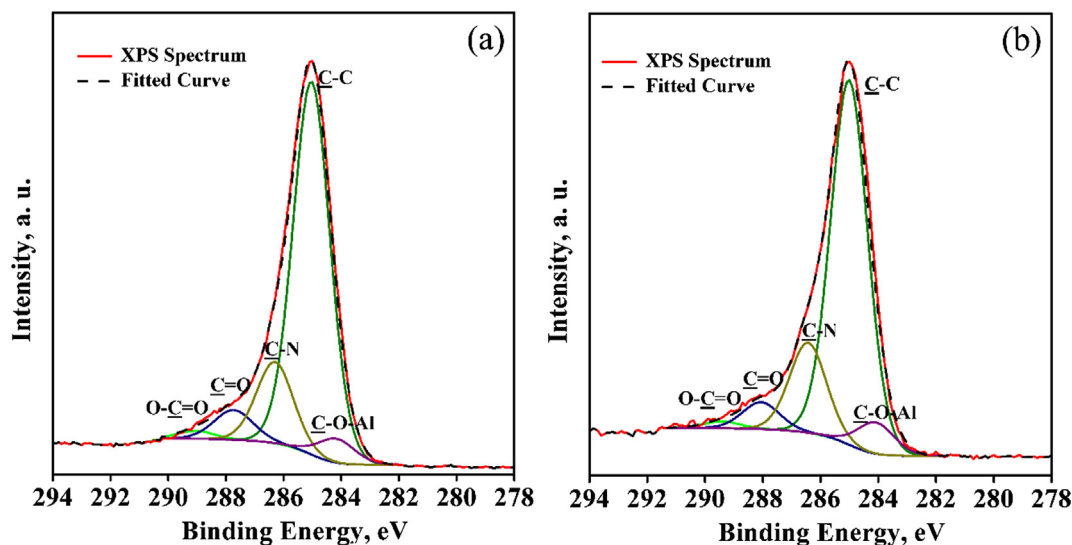


Fig. 7. C1s core level spectra recorded as a function of Al coating: (a) 0.8 nm and (b) 3.2 nm.

understand the seemingly contradictory results in the literature. Nagatsuka et al. showed that CFRP (PPS) could not be directly welded onto 304 stainless steel by FLW. In contrast, a research group in Germany showed that CFRP (PPS) was successfully joined to magnesium alloys and aluminum alloys using refill friction stir welding (RFSSW). During FLW, the metal at the joining interface did not

experience plastic deformation. The joint strength of dissimilar metal welds produced by FLW highly depended on the chemical bonds formed across the interface. Owing to the absence of polar functional groups in PPS, C–O–M bonds could not form at the interface of PPS and stainless steel to provide joints strength. High-temperature plastic deformation occurred in the metals at joining interface during RFSSW. Mechanical

Table 5

A summary of the weldability of metal and polymer combinations according to available literature.

Authors	Polymers	Metals	Welding methods	C=O groups	Specific surface modification
Liu et al. [3]	PA6	6061 Al	FLW	Yes	No
Liu et al. [5]	PA6	AZ31B Mg	FLW	Yes	No
Liu et al. [4]	PE	Non-combustible Mg	FLW	No	Corona discharge
Nagatsuka et al. [30]	CFRP-PA6	5052Al	FLW	Yes	No
Nagatsuka et al. [16]	PA 6	Low carbon steel	FLW	Yes	No
Wu et al. [7]	CFRP-PA6	Copper	FLW	Yes	No
Nagatsuka et al. [14]	CFRP-PA6	304 stainless steel	RSW	Yes	No
Nagatsuka et al. [14]	CFRP-PPS	304 stainless steel	RSW	No	Coupling agent
Nagatsuka et al. [14]	CFRP-PP	304 stainless steel	RSW	No	Acid-modified
Ageorges et al. [31]	PEI	7075 Al	RSW	Yes	No
Katayama et al. [6]	PET	304 stainless steel	LDJ	Yes	No
Kawahito et al. [32]	PET	Zr55Al10Ni5Cu30	LDJ	Yes	No
Farazila et al. [27]	PET	copper	LDJ	Yes	No
Farazila et al. [27]	PET	5052 Al	LDJ	Yes	No
Wahba et al. [33]	PET	AZ91D Mg	LDJ	Yes	No
Jung et al. [34]	CFRP-PA6	304 stainless steel	LDJ	Yes	No
Jung et al. [35]	CFRP-PA6	Galvanized steel	LDJ	Yes	No
Yusof et al. [36]	PET	5052Al	LDJ	Yes	No
Hussein et al. [37,38]	PMMA	304 stainless steel	LDJ	Yes	No
Lambiase et al. [9]	PC	304 stainless steel	LDJ	Yes	No
Zhang et al. [39]	CFRP-PA6	6061Al	LDJ	Yes	No
Ai et al. [40]	PET	Ti6Al4V	LDJ	Yes	No
Chan at al. [41]	PET	CP Ti	LDJ	Yes	No
Jung et al. [28]	ABS	Galvanized steel	LDJ	No	Surface oxidation
Yusof et al. [42]	PET	5052Al	FAW	Yes	No
Amancio et al. [43]	CFRP-PPS	AZ31 Mg	RFSSW	No	Acetone rinsing
Goushegir et al. [44]	CFRP-PPS	2024 Al	RFSSW	No	Acetone rinsing
Esteves et al. [45]	CFRP-PPS	6181 Al	RFSSW	No	Acetone rinsing
Balle et al. [46]	CFRP-PA66	1050Al	USW	Yes	No
Balle et al. [13]	CFRP-PA66	5754Al	USW	Yes	No
Lionetto et al. [12]	CFRP-PA6	5754Al	USW	Yes	No
Lambiase et al. [29]	PEEK	5053Al	FAW	Yes	Laser texturing
Lambiase et al. [21]	PVC	5053Al	FAW	No	Laser texturing

Nomenclature: FLW (Friction lap welding); RSW (Resistance spot welding); LDJ (Laser direct joining); FAW (Friction assisted welding); RFSSW (Refill friction stir spot welding); USW (Ultrasonic spot welding); PA6 (Polyamide6); PE (Polyethylene); CFRP-PA6 (Carbon fiber reinforced plastic with Polyamide6 as matrix); CFRP-PPS (Carbon fiber reinforced plastic with poly phenylene sulfide as matrix); CFRP-PP (Carbon fiber reinforced plastic with polypropylene as matrix); PEI (Polyetherimide); PET (Polyethylene terephthalate); PMMA (Polymethylmethacrylate); PC (Polycarbonate); ABS (Acrylonitrile butadiene styrene); CFRP-PA66 (Carbon fiber reinforced plastic with Polyamide66 as matrix); PEEK (Polyether ether ketone); PVC (Polyvinylchloride).

interlocking between carbon fiber and the plastically deformed metal developed after RFSSW, allowing the hybrid joints produced by RFSSW have some degree of load bearing capability.

5. Conclusions

After XPS analysis of the PA66 plates with varying thickness (i.e., 0.8–3.2 nm) of alumina coating, both Al2p and C1s spectra confirmed Al–O–C bonds develop at the interface between PA66 and alumina coating. Approximately 23.6% of the Al atoms in the 0.8 nm alumina coating have involved in Al–O–C bonds. A very low ratio (< 3%) of Al–C bond was individualized in Al2p spectra, but no Al–C bond can be distinguished in C1s spectra due to the low volume of such bond across the interface. The present experiment has shown that the C=O groups on PA66 surface enabled the development C–O–Al bonds when alumina was deposited onto PA66 plates, providing strong support that the formation of Al–O–C bonds at the welding interface is the key mechanism for producing strong metal/polymer dissimilar material welds by FLW.

Acknowledgments

This work was performed in part at the University of Michigan Lurie Nanofabrication Facility. KS acknowledges the financial support of the University of Michigan College of Engineering and NSF grant #DMR-0420785, and technical support from the Michigan Center for Materials Characterization. FL and PD acknowledge the financial support made available by the National Research Foundation of Korea (NRF) Grant through GCRC-SOP at University of Michigan under Project 2-1: Reliability and Strength Assessment of Core Parts and Material System.

References

- L.D.R. Grant, R.D. Adams, L.F.M. da Silva, Effect of the temperature on the strength of adhesively bonded single lap and T joints for the automotive industry, *Int. J. Adhes. Adhes.* 29 (5) (2009) 535–542.
- A. Pramanik, A.K. Basak, Y. Dong, P.K. Sarker, M.S. Uddin, G. Littlefair, A.R. Dixit, S. Chattopadhyaya, Joining of carbon fibre reinforced polymer (CFRP) composites and aluminium alloys - a review, *Compos. Part A-Appl. Sci.* 101 (2017) 1–29.
- F.C. Liu, J. Liao, K. Nakata, Joining of metal to plastic using friction lap welding, *Mater. Des.* 54 (2014) 236–244.
- F.C. Liu, J. Liao, Y. Gao, K. Nakata, Effect of plasma electrolytic oxidation coating on joining metal to plastic, *Sci. Technol. Weld Joining* 20 (4) (2015) 291–296.
- F.C. Liu, K. Nakata, J. Liao, S. Hirota, H. Fukui, Reducing bubbles in friction lap welded joint of magnesium alloy and polyamide, *Sci. Technol. Weld Joining* 19 (7) (2014) 578–587.
- S. Katayama, Y. Kawahito, Laser direct joining of metal and plastic, *Scr. Mater.* 59 (12) (2008) 1247–1250.
- L.H. Wu, K. Nagatsuka, K. Nakata, Direct joining of oxygen-free copper and carbon-fiber-reinforced plastic by friction lap joining, *J. Mater. Sci. Technol.* 34 (1) (2018) 192–197.
- F.C. Liu, P. Dong, W. Lu, K. Sun, Can Polymer be Welded to Metal? MS&T18, Columbus, 2018.
- F. Lambiase, S. Genna, C. Leone, A. Paoletti, Laser-assisted direct-joining of carbon fibre reinforced plastic with thermosetting matrix to polycarbonate sheets, *Opt. Laser Technol.* 94 (2017) 45–58.
- F. Lambiase, S. Genna, Laser-assisted direct joining of AISI304 stainless steel with polycarbonate sheets: thermal analysis, mechanical characterization, and bonds morphology, *Opt. Laser Technol.* 88 (2017) 205–214.
- K.W. Jung, Y. Kawahito, M. Takahashi, S. Katayama, Laser direct joining of carbon fiber reinforced plastic to aluminum alloy, *J. Laser Appl.* 25 (3) (2013).
- F. Lionetto, F. Balle, A. Maffezzoli, Hybrid ultrasonic spot welding of aluminum to carbon fiber reinforced epoxy composites, *J. Mater. Process. Technol.* 247 (2017) 289–295.
- F. Balle, D. Eifler, Statistical test planning for ultrasonic welding of dissimilar materials using the example of aluminum-carbon fiber reinforced polymers (CFRP) joints, *Materialwiss. Werkst.* 43 (4) (2012) 286–292.
- K. Nagatsuka, B. Xiao, L. Wu, K. Nakata, S. Saeki, Y. Kitamoto, Y. Iwamoto, Resistance spot welding of metal/carbon-fibre-reinforced plastics and applying silane coupling treatment, *Sci. Technol. Weld Joining* 23 (3) (2018) 181–186.
- P. Mitschang, R. Velthuis, S. Emrich, M. Kopnarski, Induction heated joining of aluminum and carbon fiber reinforced nylon 66, *J. Thermoplast. Compos.* 22 (6) (2009) 767–801.
- K. Nagatsuka, D. Kitagawa, H. Yamaoka, K. Nakata, Friction lap joining of thermoplastic materials to carbon steel, *ISIJ Int.* 56 (7) (2016) 1226–1231.
- A. Gisario, M. Mehrpouya, E. Pizzi, Dissimilar joining of transparent Poly(ethylene terephthalate) to aluminum 7075 sheets using a diode laser, *J. Laser Appl.* 29 (2) (2017).
- F. Lambiase, A. Paoletti, A. Di Ilio, Effect of tool geometry on mechanical behavior of friction stir spot welds of polycarbonate sheets, *Int. J. Adv. Manuf. Technol.* 88 (9–12) (2017) 3005–3016.
- W.S. Junior, U.A. Handge, J.F. dos Santos, V. Abetz, S.T. Amancio, Feasibility study of friction spot welding of dissimilar single-lap joint between poly(methyl methacrylate) and poly(methyl methacrylate)-SiO₂ nanocomposite, *Mater. Des.* 64 (2014) 246–250.
- K. Kondoh, J. Umeda, CO bond enhancing direct bonding strength between plastic and pure titanium, *Mater. Lett.* 211 (2018) 331–334.
- F. Lambiase, A. Paoletti, V. Grossi, A. Di Ilio, Friction assisted joining of aluminum and PVC sheets, *J. Manuf. Process.* 29 (2017) 221–231.
- A. Ringenbach, Y. Jugnet, T.M. Duc, Interfacial chemistry in Al and Cu metallization of untreated and plasma-treated polyethylene and polyethylene terephthalate, *J. Adhes. Sci. Technol.* 9 (9) (1995) 1209–1228.
- L. Sandrin, E. Sacher, X-ray photoelectron spectroscopy studies of the evaporated aluminum corona-treated polyethylene terephthalate interface, *Appl. Surf. Sci.* 135 (1–4) (1998) 339–349.
- M. Bou, J.M. Martin, T. Lemogne, Chemistry of the interface between aluminum and polyethylene terephthalate by XPS, *Appl. Surf. Sci.* 47 (2) (1991) 149–161.
- H.X. Liu, K. Wang, C. Zhang, P. Li, Y.Y. Gao, Y. Hu, X. Wang, Influence of film thickness of Ti coating on bonding quality of glass with PET, *Surf. Eng.* 28 (9) (2012) 705–709.
- G.M. Porta, J.D. Rancourt, L.T. Taylor, Interfacial interactions of titanium-coated polyester films, *Chem. Mater.* 3 (3) (1991) 423–428.
- Y. Farazila, Y. Miyashita, W. Hua, Y. Mutoh, Y. Otsuka, YAG laser spot welding of PET and metallic materials, *J. Laser Micro Nanoeng.* 6 (1) (2011) 69–74.
- D.J. Jung, J. Cheon, S.J. Na, Effect of surface pre-oxidation on laser assisted joining of acrylonitrile butadiene styrene (ABS) and zinc-coated steel, *Mater. Des.* 99 (2016) 1–9.
- F. Lambiase, A. Paoletti, Mechanical behavior of AA5053/polyetheretherketone (PEEK) made by Friction Assisted Joining, *Compos. Struct.* 189 (2018) 70–78.
- K. Nagatsuka, S. Yoshida, A. Tsuchiya, K. Nakata, Direct joining of carbon-fiber-reinforced plastic to an aluminum alloy using friction lap joining, *Compos. Part B-Eng.* 73 (2015) 82–88.
- C. Ageorges, L. Ye, Resistance welding of metal/thermoplastic composite joints, *J. Thermoplast. Compos.* 14 (6) (2001) 449–475.
- Y. Kawahito, Y. Niwa, T. Terajima, S. Katayama, Laser direct joining of glassy metal Zr₅₅Al₁₆Ni₅Cu₃₀ to engineering plastic polyethylene terephthalate, *Mater. Trans.* 51 (8) (2010) 1433–1436.
- M. Wahba, Y. Kawahito, S. Katayama, Laser direct joining of AZ91D thixomolded Mg alloy and amorphous polyethylene terephthalate, *J. Mater. Process. Technol.* 211 (6) (2011) 1166–1174.
- K.W. Jung, Y. Kawahito, S. Katayama, Laser direct joining of carbon fibre reinforced plastic to stainless steel, *Sci. Technol. Weld Joining* 16 (8) (2011) 676–680.
- K.W. Jung, Y. Kawahito, M. Takahashi, S. Katayama, Laser direct joining of carbon fiber reinforced plastic to zinc-coated steel, *Mater. Des.* 47 (2013) 179–188.
- F. Yusof, M. Yukio, M. Yoshiharu, M.H.A. Shukor, Effect of anodizing on pulsed Nd:YAG laser joining of polyethylene terephthalate (PET) and aluminium alloy (A5052), *Mater. Des.* 37 (2012) 410–415.
- F.I. Hussein, E. Akman, B.G. Oztoprak, M. Gunes, O. Gundogdu, E. Kacar, K.I. Hajim, A. Demir, Evaluation of PMMA joining to stainless steel 304 using pulsed Nd:YAG laser, *Opt. Laser Technol.* 49 (2013) 143–152.
- F.I. Hussein, K.N. Salloomi, E. Akman, K.I. Hajim, A. Demir, Finite element thermal analysis for PMMA/st.st.304 laser direct joining, *Opt. Laser Technol.* 87 (2017) 64–71.
- Z. Zhang, J.G. Shan, X.H. Tan, Evaluation of the CFRP grafting and its influence on the laser joining CFRP to aluminum alloy, *J. Adhes. Sci. Technol.* 32 (4) (2018) 390–406.
- Y.W. Ai, K. Zheng, Y.C. Shin, B.X. Wu, Analysis of weld geometry and liquid flow in laser transmission welding between polyethylene terephthalate (PET) and Ti6Al4V based on numerical simulation, *Opt. Laser Technol.* 103 (2018) 99–108.
- C.W. Chan, G.C. Smith, Fibre laser joining of highly dissimilar materials: commercially pure Ti and PET hybrid joint for medical device applications, *Mater. Des.* 103 (2016) 278–292.
- F. Yusof, Y. Miyashita, N. Seo, Y. Mutoh, R. Moshwan, Utilising friction spot joining for dissimilar joint between aluminium alloy (A5052) and polyethylene terephthalate, *Sci. Technol. Weld Joining* 17 (7) (2012) 544–549.
- S.T. Amancio, C. Bueno, J.F. dos Santos, N. Huber, E. Hage, On the feasibility of friction spot joining in magnesium/fiber-reinforced polymer composite hybrid structures, *Mater. Sci. Eng. A-Struct.* 528 (10–11) (2011) 3841–3848.
- S.M. Goushegir, J.F. dos Santos, S.T. Amancio, Friction Spot Joining of aluminum AA2024/carbon-fiber reinforced poly(phenylene sulfide) composite single lap joints: Microstructure and mechanical performance, *Mater. Des.* 54 (2014) 196–206.
- J.V. Esteves, S.M. Goushegir, J.F. dos Santos, L.B. Canto, E. Hage, S.T. Amancio, Friction spot joining of aluminum AA6181-T4 and carbon fiber-reinforced poly(phenylene sulfide): effects of process parameters on the microstructure and mechanical strength, *Mater. Des.* 66 (2015) 437–445.
- F. Balle, G. Wagner, D. Eifler, Ultrasonic spot welding of aluminum sheet/carbon fiber reinforced polymer-joints, *Materialwiss. Werkst.* 38 (11) (2007) 934–938.